Electronic Structures and Spectroscopic Properties of Mono- and Binuclear d^8 Complexes: A Theoretical Exploration on Promising Phosphorescent Materials

Qing-Jiang Pan,[†,‡] Hong-Xing Zhang,*[,†] Xin Zhou,[†] Hong-Gang Fu,[‡] and Hai-Tao Yu[‡]

State Key Laboratory of Theoretical and Computational Chemistry, Institute of Theoretical Chemistry, Jilin University, Changchun 130023, China, and School of Chemistry and Materials Science, Heilongjiang University, Haerbin 150080, China

Received: August 10, 2006; In Final Form: September 29, 2006

The structures of *trans*-$[M_2(CN)_4(PH_2CH_2PH_2)_2]$ (M = Pt (**1**), Pd (**2**), and Ni (**3**)), *trans*-$[Pt_2X_4(PH_2CH_2PH_2)_2]$ (X = Cl (**4**) and Br (**5**)), and *trans*-$[M(CN)_2(PH_3)_2]$ (M = Pt (**6**), Pd (**7**), and Ni (**8**)) in the ground state were optimized using the MP2 method. Frequency calculations reveal that the weak metal−metal interaction is essentially attractive for **1**, **2**, **4**, and **5** but not for **3**. The TD-DFT calculations associated with the polarized continuum model (PCM) were performed to predict absorption spectra in CH_2Cl_2 solution. Experimental spectra are well reproduced by our results. With respect to analogous mononuclear d^8 complexes (**6**−**8**), a large red shift of the absorption wavelength was calculated for the binuclear d^8 complexes (**1**−**3**). Relative to **1** with unsaturated CN^- donors, introduction of saturated halogen donors into **4** and **5** changes their electronic structures, especially the HOMO and LUMO. The TD-DFT and subsequent unrestricted MP2 calculations predict that **1** produces the lowest-energy d → p emission while **2**−**5** favor the d → d emissions, agreeing with experimental observations.

1. Introduction

Study on the luminescence of d^8 complexes has attracted growing attention in the last few decades, which is in part due to the interesting observation of weak metal−metal interactions.[1−3] A number of d^8 complexes with well-defined metal−metal distances have been reported.[4] Special attention has been focused on their unique absorption and emission spectra. For example, Pt(II) α-diimine complexes often crystallize in linear-chain structures in which Pt(II)−Pt(II) distances range from 3.0 to 3.5 Å, leading to stronger perturbation on the luminescence.[5−9]

One approach to probe the role of metal−metal interaction in determining the spectroscopic properties of the d^8 square-planar complexes involves the design and synthesis of discrete molecules with known metal−metal distances.[10−15] Che and co-workers[12−15] synthesized a series of binuclear d^8 complexes, *trans*-$[M_2(CN)_4(PR_2CH_2PR_2)_2]$ (M = Pt, Pd, and Ni; R = Me and Cy) and *trans*-$[M_2(CN)_4(PPh_2CH_2PPh_2)_2]$ (M = Pt and Pd). These discrete binuclear M(II) dimers possess intramolecular M(II)−M(II) distances of 2.9−3.3 Å.[12−15] Among these, the platinum(II) complex exhibits intense emission in both the solid state and solution at room temperature in the visible region, which has been assigned as a σ(p) → σ^*(d) (metal-centered, MC) transition,[12,13,16] while the palladium(II) and nickel(II) analogues do not produce MC transition emissions under the same conditions.[12−16]

In the early 1980s, the discovery of $[Pt_2(pop)_4]^{4-}$ (pop^{2-} = $P_2O_5H_2^{2-}$)[1,2] with rich photophysical and photochemical properties greatly motivated studies of binuclear d^8 complexes. The light-induced $^3A_{2u}$ excited state of $[Pt_2(pop)_4]^{4-}$ is highly reactive. It reacts with a wide range of quenchers by mechanisms that involve the platinum complex as an oxidant, reductant, or atom-transfer reagent. Understanding the electronic structures of binuclear d^8 complexes originates from simple molecular orbital theory.[17] The featured absorption and emission were attributed to the metal-localized σ^*(d) → σ(p) transition. Recently, density functional theory (DFT) methods have been used to explore such complexes.[18] The Pt−Pt distances of $[Pt_2(pop)_4]^{4-}$ calculated by Coppens[18a] and Rillema[18b] are 3.04 and 2.82 Å in the ground and triplet excited states, respectively, compared with 2.92 and 2.64−2.71 Å determined by experiments.[1,2,19] Similarly, the authors related the lowest energy emission to the σ(p) → σ^*(d) transition.

Since the presence of a bridging ligand facilitates the intramolecular interaction,[20−22] *trans*-$[M_2(CN)_4(PR_2CH_2PR_2)_2]$ (M = Pt, Pd, and Ni; R = Me, Ph, and Cy) with the eight-membered ring conformation[12−15] can serve as an ideal candidate for investigations on the relationship between spectroscopic properties and d^8−d^8 interaction. While there are some reports about the electronic structures of d^8 complexes in the ground state,[18,23−26] few attempts on the excited-state properties of a series of Pt(II), Pd(II), and Ni(II) complexes have been made.

In this paper, the ground- and excited-state properties of *trans*-$[M_2(CN)_4(PH_2CH_2PH_2)_2]$ (M = Pt (**1**), Pd (**2**), and Ni (**3**)), *trans*-$[Pt_2X_4(PH_2CH_2PH_2)_2]$ (X = Cl (**4**) and Br (**5**)), and *trans*-$[M(CN)_2(PH_3)_2]$ (M = Pt (**6**), Pd (**7**), and Ni (**8**)) were explored theoretically (Figure 1). With variation of the metal atoms (**1**−**3** and **6**−**8**) and donating ligands (**1**, **4**, and **5**), the present calculations provide insight into the electronic properties of the d^8 complexes.

2. Computational Details and Theory

We used *trans*-$[M_2(CN)_4(PH_2CH_2PH_2)_2]$ as a computational model to represent the real complexes, *trans*-$[M_2(CN)_4(PR_2CH_2PR_2)_2]$ (R = Me, Ph, and Cy).[12−15] A similar model has been applied in many works using hydrogen to replace methyl, phenyl, cyclohexyl, etc., heavy substituents.[12,14,21,22,27] The C_{2h}

[†] Jilin University.
[‡] Heilongjiang University.

10.1021/jp065183b CCC: $37.00
Published on Web 12/22/2006

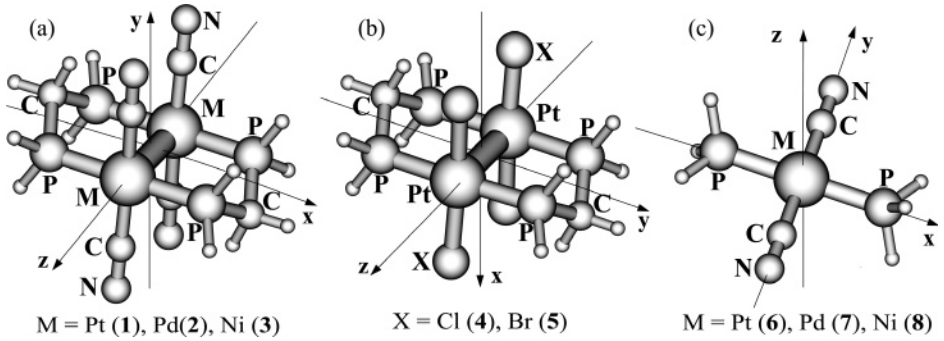

Figure 1. Geometry structures of *trans*-$[M_2(CN)_4(PH_2CH_2PH_2)_2]$ (M = Pt (**1**), Pd (**2**), and Ni (**3**)), *trans*-$[Pt_2X_4(PH_2CH_2PH_2)_2]$ (X = Cl (**4**) and Br (**5**)), and *trans*-$[M(CN)_2(PH_3)_2]$ (M = Pt (**6**), Pd (**7**), and Ni (**8**)).

TABLE 1: Optimized Geometry Parameters of *trans*-$[M_2(CN)_4(PH_2CH_2PH_2)_2]$ (M = Pt (1), Pd (2), and Ni (3)) and *trans*-$[Pt_2X_4(PH_2CH_2PH_2)_2]$ (X = Cl (4) and Br (5)) Using the MP2 Method for the Ground State and the UMP2 Method for the Triplet Excited State Together with the Experimental Values from X-ray Diffraction[a]

	1			**2**			**3**		**4**		**5**	
params[b]	^1A_g	exp.	^3A_u	^1A_g	exp.	^3A_u	^1A_g	exp.	^1A_g	^3B_g	^1A_g	^3B_g
						bond lengths (Å)						
M−M	3.069	3.057	2.794	3.020	3.043	2.753	3.021	2.957	3.166	3.144	3.164	3.062
M−P	2.305	2.329	2.343	2.292	2.345	2.356	2.116	2.236	2.300	2.356	2.300	2.332
M−Y	2.020	1.994	2.025	2.005	2.001	2.024	1.826	1.864	2.345	2.373	2.481	2.531
C≡N	1.221	1.161	1.171	1.222	1.140	1.228	1.223	1.149				
P···P	3.065		3.097	3.069		3.095	3.069		3.067	3.093	3.067	2.981
						bond angles (deg)						
P−M−P	179.9	177.3	172.6	178.8	177.2	171.7	178.7	176.5	177.5	178.8	177.6	178.0
P−M−M	89.9	90.2	93.7	90.6	90.0	94.1	90.7	90.9	88.8	89.4	88.8	89.0
Y−M−Y	173.5	176.6	173.8	172.2	176.6	172.6	170.9	175.8	172.1	177.1	167.3	165.5
Y−M−M	93.2	92.1	93.1	93.9	91.7	93.7	94.5	92.0	94.0	91.5	96.3	97.2
Y−M−P	92.7	94.7	92.7	93.1	94.7	93.2	92.4	89.9	93.4	93.0	92.8	93.1
Y−M−P	87.3	88.8	86.9	86.8	88.7	86.3	87.5	85.5	86.7	87.0	87.4	87.1

[a] Experimental values of *trans*-$[M_2(CN)_4(PCy_2CH_2PCy_2)_2]$ (M = Pt, Pd, and Ni) from refs 12 and 14. [b] Y atom denotes the C atom of the cyanide group for **1**−**3**, the Cl atom for **4**, and the Br atom for **5**.

symmetry was adopted to settle the conformations of the binuclear d^8 metal complexes (**1**−**5**). Structures in the ground and lowest energy triplet excite states were optimized by second-order Møller−Plesset perturbation (MP2)[28] and unrestricted MP2 (UMP2) methods, respectively. Subsequent frequency calculations provide deep insight into the d^8−d^8 interactions.

It has been well established that the transition energies calculated by the time-dependent density functional theory (TD-DFT) method are comparable in accuracy to those by the higher level configuration interaction methods.[29−32] Therefore, we estimated absorption spectra of **1**−**5** at the TD-DFT level with the B3LYP functional[31−33] on the basis of the ground-state structures. Because calculations on the single molecule only correspond to the behavior in the gas phase, the polarized continuum model (PCM)[34] was employed to account for the CH_2Cl_2 solvent effects. To explore the influence of M(II)−M(II) interaction on electronic transitions, the reference molecules (**6**−**8**) keeping the C_{2h} symmetry in the gas phase and solution were studied using the same methods as those of **1**−**5**.

In the calculations the effective core potentials (ECPs) of Hay and Wadt[35] were used for Pt, Pd, Ni, Cl, Br, and P atoms with 18, 18, 18, 7, 7, and 5 valence electrons, respectively. The LANL2DZ basis sets associated with the ECPs were adopted for all atoms. To describe the metal−metal interaction and the molecular properties precisely[22,36] one additional function was implemented for Pt ($\alpha_f = 0.18$), Pd ($\alpha_f = 0.2$), Ni ($\alpha_f = 0.22$), Cl ($\alpha_d = 0.514$), Br ($\alpha_d = 0.389$), and P ($\alpha_d = 0.34$).[36a−c] All calculations were accomplished by using the Gaussian03 package[37] on an Origin/3900 server.

TABLE 2: Optimized Geometry Parameters of *trans*-$[M(CN)_2(PH_3)_2]$ (M = Pt (6), Pd (7) and Ni (8)) Using the MP2 Method for the ^1A_g Ground State, Together with the Experimental Values from X-ray Diffraction[a]

	6		**7**	**8**	
params	^1A_g	exp.	^1A_g	^1A_g	exp.
		bond lengths (Å)			
M−P	2.320	2.336	2.310	2.125	2.243
M−C	2.021	2.021	2.010	1.824	1.857
C≡N	1.220	1.106	1.221	1.220	1.148
		bond angles (deg)			
C−M−P	88.5	89.2	88.1	88.0	89.0
C−M−P	91.5	90.8	92.0	92.0	91.0

[a] Experimental values of *trans*-$[M(CN)_2(PCy_3)_2]$ (M = Pt and Ni) from ref 12.

3. Results and Discussion

3.1. Ground-State Structures. The MP2 optimizations were performed for the ground-state structures of **1**−**8** keeping the C_{2h} symmetry (Figure 1). These d^8 complexes all have ^1A_g ground electronic state. The optimized main geometry parameters are presented in Tables 1 and 2. For comparison, we also list X-ray crystal diffraction data of *trans*-$[M_2(CN)_4(PCy_2CH_2PCy_2)_2]$ (M = Pt, Pd, and Ni) and *trans*-$[M(CN)_2(PCy_3)_2]$ (M = Pt and Ni).[12,13] The calculated results show that two M(II) atoms and two bridging phosphine ligands of dimers (**1**−**5**) form an eight-membered ring skeleton, and two cyanide/halide ions bond to each M(II) atom. Each divalent metal atom exhibits square-planar tetracoordination with two *trans*-cyano groups and two *trans*-phosphorus atoms from the phosphine ligands. The calculated P−M−P angles of ca. 178° and Y−M−Y angles of

TABLE 3: Calculated Absorptions of 1 in CH_2CL_2 Solution at the TD-DFT (B3LYP) Level, Associated with the Absorptions Observed in the Experiment[a]

		$PR_2C\ H_2PR_2$ (R = H)				Me		Ph		Cy	
states	conf.	|CI coef.| > 0.2	trans. energy (nm)	trans. energy (eV)	f[b]	λ_{max}	ϵ_{max}	λ_{max}	ϵ_{max}	λ_{max}	ϵ_{max}
^3A_u	$15a_u \rightarrow 19\ a_g$	0.726	392	3.16	0.000	375	50	390		388	300
A ^1A_u	$15a_u \rightarrow 19\ a_g$	0.676	338	3.66	0.215	328	24300	324	10 500	337	24 100
B ^1A_u	$15a_u \rightarrow 20\ a_g$	0.684	285	4.35	0.004						
C ^1B_u	$18b_u \rightarrow 19a_g$	0.686	276	4.49	0.077	256	6000	275 (sh)[c]	9690	263	8900
D ^1B_u	$15b_g \rightarrow 16a_u$	0.644	266	4.67	0.002						
	$18b_u \rightarrow 20a_g$	−0.234									
E ^1B_u	$17b_u \rightarrow 19a_g$	0.695	248	5.00	0.003	235	6000	228 (sh)[c]	50 450		
F ^1B_u	$16b_u \rightarrow 19a_g$	0.640	228	5.44	0.001						
	$18b_u \rightarrow 20a_g$	0.260									
G ^1B_u	$18b_u \rightarrow 20a_g$	0.595	226	5.48	0.003						
	$16b_u \rightarrow 19a_g$	−0.280									
	$15b_g \rightarrow 16a_u$	0.229									

[a] Absorption spectra in CH_2Cl_2 solution for *trans*-$[Pt_2(CN)_4(PR_2CH_2PR_2)_2]$ (R = Me, Ph and Cy) from refs 12 and 13. [b] Oscillator strength. [c] Shoulder band observed in experiment.

ca. 172° for **1**−**5** are comparable to experimental values of 177° and 176°, respectively (Table 1, the Y atom denotes the C atom of the cyanide group for **1**−**3**, the Cl atom for **4**, and the Br atom for **5**). For the platinum(II) dimers (**1**, **4**, and **5**), the Y−Pt−Y angles were calculated at 173.5°, 172.1°, and 167.3°, respectively. Among these, the Br−Pt−Br angle of **5** has the largest 12.7° deviation from 180° to decrease the repulsion of the two large Br atoms as much as possible. A similar case occurs in crystals of *trans*-$[Pd_2X_4(PMe_2CH_2PMe_2)_2]$ (X = CN, Cl, and Br), where the X−Pd−X angles are 174.0°,[14] 173.1°,[4g] and 168.3°,[4g] respectively. The two MP_2Y_2 units in **1**−**5** are in normal face-to-face orientation reflected in Figure 1a and 1b. With respect to monomers **6**−**8**, we predict the P−M−P and C−M−C angles to be 180° just like experimental reports.[12]

It can be seen from Tables 1 and 2 that the calculated M−P, M−Y, and C≡N distances are in agreement with the corresponding experimental values. The largest differences of these distances are ca. 0.08 (M−P), 0.04 (M−Y), and 0.11 Å (C≡N) for **3**, **3**, and **6**, respectively. It is thought that these differences result from the use of relatively smaller basis sets (P(2s2p1d), N(3s2p), C(3s2p), and H(2s)) and approximation of H atoms in place of Me, Ph, and Cy groups. To examine the dependence of the C≡N bond length on basis sets, we optimized the HCN molecule at the MP2 level. With the increase of the basis sets (LanL2DZ, 6-31G*, 6-311G**, 6-311G (3df, 3pd)), the C≡N distance is improved greatly from 1.212 to 1.178 to 1.165 Å. Use of larger basis sets makes the calculated C≡N distance very close to the experimental value of 1.161 Å.

An interesting feature in the binuclear metal complexes is the weak metal−metal interaction.[1,2,10−16] Previous studies on related Au(I) complexes showed that the Au(I)−Au(I) distance falls within the range of 2.8−3.2 Å and that the energy of this interaction is comparable to that of hydrogen bonds.[20−22,36,38,39] Here, the calculated M(II)−M(II) distances for **1**−**3** in the ground state range from 3.020 to 3.069 Å, in agreement with ca. 3.0 Å (mean value) for *trans*-$[M_2(CN)_4(PCy_2CH_2PCy_2)_2]$ (M = Pt, Pd, and Ni),[12−15] and the Pt(II)−Pt(II) distances for **4** and **5** are 3.166 and 3.164 Å, respectively. For the platinum(II) complexes, the longer Pt(II)−Pt(II) distances of **4** and **5** relative to **1** are related to the larger repulsion of two halogen atoms, which has been reflected in the Y−M−M angles (94.0° for Cl−Pt−Pt, 96.3° for Br−Pt−Pt, and 93.2° for C−Pt−Pt) as shown in Table 1. The slightly shorter M(II)−M(II) distance than the van der Waals contacts of 3.2 Å[40] implies that a possible weak bonding interaction between the two M(II) centers in **1**−**5** occurs. To judge whether the interaction is bonding or not, we carried out the frequency calculations on **1**−**5** at the MP2 level.

TABLE 4: Calculated Absorptions of 6 in CH_2CL_2 Solution at the TD-DFT (B3LYP) Level

states	conf.	|CI coef.| > 0.2	trans. energy (nm)	trans. energy (eV)	f
^3A_u	$12a_g \rightarrow 4a_u$	0.723	264	4.69	0.000
A ^1B_u	$4b_g \rightarrow 4a_u$	0.673	249	4.98	0.090
B ^1A_u	$11a_g \rightarrow 4a_u$	0.688	239	5.18	0.001
C ^1A_u	$12a_g \rightarrow 4a_u$	0.672	233	5.32	0.070
D ^1B_u	$11b_u \rightarrow 13a_g$	0.524	208	5.96	0.027
	$3b_g \rightarrow 4a_u$	−0.468			
E ^1B_u	$3b_g \rightarrow 4a_u$	0.497	198	6.26	0.217
	$11b_u \rightarrow 13a_g$	0.432			
F ^1B_u	$10b_u \rightarrow 13a_g$	0.668	195	6.35	0.124

It is shown that the frequencies at 94, 106, 83, and 75 cm^{-1} were attributed to M(II)−M(II) stretching vibrations for **1**, **2**, **4**, and **5**, respectively. Among these, the calculated value of **1** is comparable to a resonance-enhanced band at 93 cm^{-1} from resonance Raman spectra of *trans*-$[Pt_2(CN)_4(PCy_2CH_2PCy_2)_2]$.[12] However, despite carefully examining all the vibrational modes, no Ni−Ni stretching vibration is found for **3**. Our frequency calculations demonstrate that the weak metal−metal interaction in **1**, **2**, **4**, and **5** is bonding in nature, but in **3** is not. The present calculated results support experimental investigations on *trans*-$[M_2(CN)_4(PR_2CH_2PR_2)_2]$ (M = Pt, Pd, and Ni; R = Me and Cy),[12,14] which demonstrated the existence of weak metal−metal bonding interaction in platinum and palladium complexes but no bonding interaction in nickel complex.

3.2. Electronic Structures and Absorption Spectra. On the basis of the ground-state structures, TD-DFT (B3LYP) associated with the PCM solvent-effect model was performed to predict the absorption spectra of **1**−**8** in CH_2Cl_2 solution. With respect to the ^1A_g ground state under the C_{2h} point group, the $^1A_g \rightarrow {}^1A_u$ and $^1A_g \rightarrow {}^1B_u$ transitions are dipole allowed. We summarize the calculated low-lying absorptions in CH_2Cl_2 solution in Tables 3 and 4 and Supporting Information Tables 1−6 together with corresponding experimental data.[12−15] The detailed molecular orbital information under the TD-DFT/PCM calculations is listed in Supporting Information Tables 7−14. The coordinate orientation is depicted in Figure 1, where the *z* axis goes through the two metal atoms for dimers and is taken normal to the molecular plane for monomers.

*3.2.1. Molecular Orbitals of **1** and **6**.* It is found in Supporting Information Table 8 and Supporting Information Figure 1 that the occupied orbitals of **6** have significant Pt 5d character, accompanied by participation of the CN^- group. $3b_g$, $11a_g$, $12a_g$, and $4b_g$ (HOMO) molecular orbitals (MOs) are mainly formed

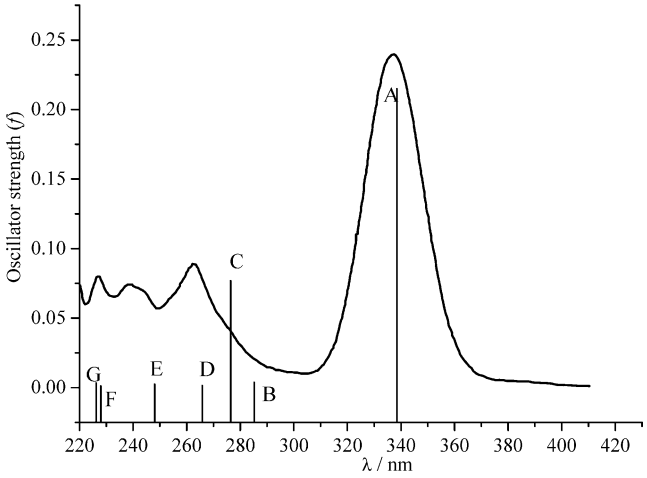

Figure 2. Calculated absorption transitions of **1** at the TD-DFT/PCM level together with experimental spectrum of *trans*-$[Pt_2(CN)_4(PCy_2CH_2PCy_2)_2]$ in CH_2Cl_2 solution (ref 12).

by 93% d_{xz}, 36% d_{xy}, 82% d_{z^2}, and 53% d_{yz}, respectively. $3a_u$ and $11b_u$ orbitals are the ligand-occupied MOs. For the metal−ligand bonding orbitals, $9b_u$, $10a_g$, and $10b_u$ MOs have the Pt−P, Pt−C, and Pt−C σ-bonding characters, respectively, while $9a_g$ and $2b_g$ MOs are d(Pt)−p(CN) π-bonding orbitals. As suggested in many studies on the electronic structures for mononuclear d^8 complexes,[25,26] the Pt $d_{x^2-y^2}$ ($13a_g$ MO) has the highest energy of the five d orbitals (Supporting Information Table 8). The p_z(Pt) mixed with some p_z(CN) and p_z(P) character forms the LUMO ($4a_u$), agreeing with the previous proposal that the π-acceptor d^8 complexes have empty orbitals with an admixture of the metal $(n+1)p_z$ and ligand-based π character.[25]

With respect to dimeric **1**, the Pt(II)−Pt(II) interaction strongly modifies the original orbitals of monomeric **6**. Most orbitals in **1** can be assigned as a single-bonding function as seen in Supporting Information Table 7 and Supporting Information Figure 1. Interactions of the d_{xy}(Pt) AOs form the δ and δ* bonds in $18a_g$ and $14a_u$ MOs, respectively. The π orbitals come from d_{xz}(Pt) and d_{yz}(Pt) AOs to give d_{xz} π ($15b_u$) and π* ($12b_g$) as well as d_{yz} π ($18b_u$) and π* ($15b_g$) orbitals. It is worth noting that there is much π(C≡N) bonding contribution to metal d_{yz} π and d_{xy} δ MOs but no contribution to d_{xz} π MOs. This is because there are symmetry-adapted $\pi[p_z(C{\equiv}N)]$ and $\pi[p_x(C{\equiv}N)]$ orbitals to $\pi[d_{yz}(Pt_2)]$ and $\delta[d_{xy}(Pt_2)]$, respectively. For the four metal−metal σ and σ* orbitals, $15a_u$ (HOMO) and $13a_u$ are the metal−metal σ* MOs mainly contributed by the d_{z^2}(Pt) AOs, whereas the $17a_g$ and $16a_g$ σ-bonding orbitals are mixed by the s(Pt) and d_{z^2}(Pt) AOs. There are four metal−ligand σ-bonding orbitals in the occupied orbitals. $14b_g$ and $17b_u$ MOs have the Pt−P σ-bonding character, while $16b_u$ and $13b_g$ MOs have Pt−C σ-bonding character. For lower-energy unoccupied orbitals, the p_z(Pt) interactions give rise to σ ($19a_g$) and σ* ($17a_u$), where there is ca. 11% s contribution to the σ* orbital. Two Pt $d_{x^2-y^2}$ AOs form the δ*($d_{x^2-y^2}$) and δ($d_{x^2-y^2}$) MOs in $16a_u$ (LUMO + 1) and $20a_g$ (LURMO + 2), respectively. For the two orbitals the result that δ*($d_{x^2-y^2}$) is lower in energy than δ($d_{x^2-y^2}$) seems puzzling. In fact, the σ*(Pt−P) character in the two orbitals plays a dominant role in determining the orbital order.

*3.2.2. Absorption Spectra of **1** and **6**.* We described the calculated electronic spin-allowed transitions of **1** in Figure 2 accompanied with the experimental spectrum of *trans*-$[Pt_2(CN)_4(PCy_2CH_2PCy_2)_2]$ observed in CH_2Cl_2 solution at room temperature.[12] Every transition is labeled as a capital letter related to its singlet excited state in Table 3. The theoretical transitions are in reasonable agreement with experimental measurements. The lowest energy absorption (A in Figure 2) arising from the $X^1A_g \rightarrow A^1A_u$ transition was estimated at 338 nm (3.66 eV). It has the largest oscillator strength (0.215) and should correspond to the peak with the largest molar absorbance in the experiment. In the excitation, the $15a_u \rightarrow 19a_g$ (HOMO → LUMO) configuration has the largest CI coefficient (ca. 0.676) in the wave functions, which determines the absorption character. According to Supporting Information Table 7, the 338 nm absorption was attributed to a $\sigma^*[d_{z^2}(Pt_2)] \rightarrow \sigma[p_z(Pt_2)]$ (metal-centered, MC) transition, comparable to experimental 328, 324, and 337 nm absorptions for *trans*-$[Pt_2(CN)_4(PR_2CH_2PR_2)_2]$ (R = Me, Ph, and Cy) in CH_2Cl_2 solution at room temperature, respectively.[12,13] The calculated 276 nm (4.49 eV) absorption related to the C^1B_u excited state has the admixture of $\pi[d_{yz}(Pt_2)] \rightarrow \sigma[p_z(Pt_2)]$ (MC) and $\pi(C{\equiv}N) \rightarrow \pi^*(C{\equiv}N)$ transitions, mainly contributed by the $18b_u \rightarrow 19a_g$ configuration. As shown in Table 3 and Supporting Information Table 7, the B^1A_u, D^1B_u, and G^1B_u excited states give rise to d → d transition absorptions at 285, 266, and 226 nm, respectively, while the E^1B_u and F^1B_u excited states produce absorptions related to Pt−P σ bonding. It is worth noting that combination of the $16b_u \rightarrow 19a_g$ and $18b_u \rightarrow 20a_g$ configurations contributes to the 228 (5.44 eV) and 226 (5.48 eV) nm absorptions just with different CI coefficients. Since the two absorptions have the same ^1B_u excited-state symmetry and very close transition energy, they should correspond to one absorption band in the experiment. Table 3 indicates that the calculated oscillator strength of absorption is correlated with the molar absorbance (ϵ_{max}) in experiments, especially for *trans*-$[Pt_2(CN)_4(PR_2CH_2PR_2)_2]$ (R = Me and Cy). Thus, the oscillator strength, to some extent, can be used to theoretically predict the experimental absorption intensity.[18b,41,42]

With respect to monomer **6**, four low-lying d → p absorptions in CH_2Cl_2 solution were calculated at 249, 239, 233, and 198 nm, corresponding to $d_{yz}(Pt) \rightarrow p_z(Pt)$, $d_{xy}(Pt) \rightarrow p_z(Pt)$, $d_{z^2}(Pt) \rightarrow p_z(Pt)$, and $d_{xz}(Pt) \rightarrow p_z(Pt)$ transitions, respectively. The lowest energy 249 nm absorption with $d_{yz}(Pt) \rightarrow p_z(Pt)$ in **6** red shifts to 276 nm with $\pi[d_{yz}(Pt_2)] \rightarrow \sigma[p_z(Pt_2)]$ in **1**. The Pt(II)−Pt(II) interaction is included in the latter. The calculated 233 nm absorption for **6** contributed by $d_{z^2}(Pt) \rightarrow p_z(Pt)$ corresponds to 338 nm for **1**. It is the strong d_{z^2}–d_{z^2} and p_z–p_z interactions in dimer **1** that result in a ca. 100 nm red shift of the absorption wavelength with respect to **6**. Comparison of the absorptions of **1** and **6** indicates that the Pt(II)−Pt(II) interaction strongly lowers the d → p transition energies, especially the $d_{z^2} \rightarrow p_z$ transition. In addition, the Pt−Pt interaction also raises the intensity of the $d_{z^2} \rightarrow p_z$ transition from 0.070 oscillator strength of **6** to 0.215 of **1**. These results agree with the corresponding experimental observations.[12]

In the TD-DFT calculations on **1**, triplet excited states related to spin-forbidden absorptions are also considered. As a heavy metal element, the spin−orbit coupling of the Pt atom should be large; thus, the singlet-to-triplet transition may appear as weak tails in the absorption spectra. The lowest energy absorption from the $X^1A_g \rightarrow {}^3A_u$ transition for **1** occurs at 392 nm (3.16 eV), belonging to the $\sigma^*[d_{z^2}(Pt_2)] \rightarrow \sigma[p_z(Pt_2)]$ (MC) transition. This is the same transition character as the dipole- and spin-allowed $X^1A_g \rightarrow A^1A_u$ transition of 338 nm. It has been observed that *trans*-$[Pt_2(CN)_4(PR_2CH_2PR_2)_2]$ (R = Me, Ph, and Cy) complexes in CH_2Cl_2 solution at room temperature exhibit very weak absorptions at 375−390 nm (Table 3).[12,13]

3.2.3. Molecular Orbitals and Absorption Spectra of Other Complexes. Just like those of **1** under the TD-DFT/PCM

calculations, frontier molecular orbitals of **2** and **3** have predominant metal orbital character, i.e., occupied orbitals mainly arise from metal *n*d (d_{xy}, d_{yz}, d_{xz}, and d_{z^2}) orbitals and unoccupied orbitals from metal $nd_{x^2-y^2}$ and $(n + 1)p_z$ orbitals (Supporting Information Tables 9 and 11). Their electronic structures have little difference. For example, the orbital energies with π(C≡N) + σ(Ni−P) character ($14b_g$ and $17a_u$) in **3** are higher than those with $\delta(d_{xy}) + \pi$(C≡N) ($18a_g$) and $\delta^*(d_{xy}) + \pi$(C≡N) ($14a_u$), different from the cases in **1** and **2** (Supporting Information Tables 7, 9, and 11). The different electronic structures may lead to more participation of σ(M−P) bonding in the transitions of **3** than of **1** and **2**.

There is little difference among **6**, **7**, and **8** in the unoccupied orbitals contributed by metal $nd_{x^2-y^2}$ and $(n + 1)p_z$. Supporting Information Table 8 displays that the orbital with p_z(Pt) character ($4a_u$) in **6** forms the LUMO, lower in energy than the orbital with $d_{x^2-y^2}$(Pt) compositions ($13a_g$). However, reversed orbital order occurs in **7** and **8** as shown in Supporting Information Tables 10 and 12, respectively. This difference results from stronger relativistic effect contraction of the p_z orbital in the Pt atom than in Pd and Ni atoms.

For the platinum(II) complexes (**1**, **4**, and **5**), the different ligand X in *trans*-$[Pt_2X_4(PH_2CH_2PH_2)_2]$ causes the differences in their electronic structures. First, halogen atoms have more contribution to the $\sigma^*(d_{z^2})$-based orbitals of **4** and **5** than the CN^- group to that of **1** (Supporting Information Tables 7, 13, and 14). Second, the interactions between adjacent halogen atoms in **4** and **5** play a more significant role in determining the order of orbital energy level. For example, the orbital with $\sigma^*(d_{z^2})$ character in **1** occupies the HOMO, while the larger repulsion of $\pi[p_z(X)]$ (X = Cl and Br) changes the orbital order into $[\pi^*(d_{xz}) + \pi(X)]$ (HOMO) and $[\sigma^*(d_{z^2}) + \pi(X)]$ (HOMO-1) of **4** and **5**. Because of more $\pi[p_z(X)]$ participations in $[\pi^*(d_{xz}) + \pi(X)]$ (49% for Cl and 59% for Br) than those in $[\sigma^*(d_{z^2}) + \pi(X)]$ (13% for Cl and 29% for Br) for **4** and **5**, respectively, the orbital with $[\pi^*(d_{xz}) + \pi(X)]$ character forms the HOMO. For $13a_u$ (LUMO) and $16a_g$ (LUMO+1) in **4**, as the σ^*(Pt−P) character plays a significant role in these MOs, $\delta^*(d_{x^2-y^2})$ occupies the lower energy $13a_u$ MO, just like in **1**−**3**.

TD-DFT calculations of **2**−**5** (Supporting Information) show that d → p and d → d transitions are dominant in the absorption spectra in CH_2Cl_2 solution, agreeing with the experimental observations.[12−15] All $\sigma^*[d_{z^2}(M_2)] \rightarrow \sigma[p_z(M_2)]$ (MC) transition absorptions have larger oscillator strengths in their low-lying transitions of **2**−**5**. For **2**, the dipole-allowed lowest energy absorption of 296 nm (4.19 eV) has the 0.156 oscillator strength, contributed by the $15a_u \rightarrow 19a_g$ and $15a_u \rightarrow 20a_g$ configurations. We assigned the absorption as the $\sigma^*[d_{z^2}(Pd_2)] \rightarrow \sigma[p_z(Pd_2)]/\delta[d_{x^2-y^2}(Pd_2)]$ transitions, comparable to intense 272−291 nm absorptions for *trans*-$[Pd_2(CN)_4(PR_2CH_2PR_2)_2]$ (R = Me, Ph, and Cy).[14,15] However, this kind of transition is not clearly observed in the absorption spectra of *trans*-$[Ni_2(CN)_4(PR_2CH_2PR_2)_2]$ (R = Me and Cy),[12] although the calculated 314 nm $\sigma^*[d_{z^2}(Ni_2)] \rightarrow \sigma[p_z(Ni_2)]$ absorption for **3** has a larger oscillator strength of 0.124 as shown in Supporting Information Table 2. Therefore, the oscillator strength of absorptions alone cannot provide sufficient information to predict the intensity of experimental absorption spectra.

Comparison between monomers and dimers in the $d_{z^2} \rightarrow p_z$ electronic transitions can provide insight into the M(II)−M(II) interaction in the ground state. For monomers **6**−**8**, the calculated 233, 218, and 246 nm absorptions were assigned as spin-allowed $d_{z^2} \rightarrow p_z$ transitions, respectively, while the $\sigma^*(d_{z^2}) \rightarrow \sigma(p_z)$ transition absorptions of dimers **1**−**3** were calculated at 338, 296, and 314 nm. The 105, 78, and 68 nm red shifts of absorption wavelengths for the Pt, Pd, and Ni complexes result from the M(II)−M(II) interactions, respectively. Accordingly, similar cases occur in the spin-forbidden $d_{z^2} \rightarrow p_z$ electronic transitions for such d^8 metal complexes. Apparently, the spectroscopic studies display the existence of a weak M(II)−M(II) interaction. However, this result seems to conflict with frequency calculations that show that the Ni−Ni interaction is not bonding in nature. In fact, two such calculated results for Ni−Ni interaction are not inconsistent. Complex **3** has an eight-membered ring skeleton structure. In the structure the bridging phosphine ligands pull the two nickel(II) atoms to a closer distance, which results in the compulsive metal−metal interaction. Thus, the metal−metal interaction should be explicitly divided into compulsive and attractive (bonding) interactions. Though the Ni−Ni interaction is essentially not attractive (bonding) as stated in frequency calculations, it affects the electronic transition energies of **3**.

3.3. Excited-State Properties. Studies on the electronic excited state of molecules continue to receive intense attention in many fields such as photochemistry,[1,2,43] spectroscopy,[1,2,44−46] and molecular pharmacology.[47] Theoretical calculation is one of the most effective means, which has been widely applied to deal with such problems.[18,22,23]

We used the UMP2 method to optimize the lowest energy triplet excited states of **1**−**5**, but the attempt on **3** fails. The optimized main geometry parameters of the excited states are given in Table 1. Optimizations on **1**, **2**, **4**, and **5** predict their lowest energy triplet excited states have ^3A_u, ^3A_u, ^3B_g, and ^3B_g electronic excited states, respectively. For **1**, the Pt−Pt distance shrinks by ca. 0.28 Å on going from the ground state to the lowest energy triple excited state, the P···P distance decreases by ca. 0.03 Å, and the Pt−P bonds lengthen ca. 0.04 Å (Table 1). Because the shrinkage of Pt−Pt is much more than that of P···P, the bonding interaction between the two Pt atoms drives the Pt−Pt shrinkage. Through the resonance Raman spectral experiment of *trans*-$[Pt_2(CN)_4(PCy_2CH_2PCy_2)_2]$, Che and coworkers estimated that the Pt(II)−Pt(II) distance contracts ca. 0.11 Å upon excitation.[12] Apparently, the Pt−Pt contraction trend is reproduced by the present calculations. When electrons are promoted, the changes of the M−M, P···P, and Pt−P distances of **2**, **4**, and **5** are similar to those of **1** (Table 1). The bonding interactions between the two metal atoms in the excited states weaken the P→M dative bonds, leading to elongation of the M−P bond length.

Analyses on the wave functions of triplet excited states demonstrate that all the HOMOs of such binuclear d^8 complexes possess M−M bonding character, intuitively depicted in Figure 3. This results in stronger M−M interactions and shorter M−M distances in the triplet excited states with respect to those in the singlet ground states. The differences of the M−M distances are 0.28 (**1**) > 0.27 (**2**) > 0.10 (**5**) > 0.02 Å (**4**). This order is closely related to the repulsion between two adjacent X^- (CN^-, Cl^-, and Br^-) ligands, the donating ability of X^-, as well as the HOMO character in the excited state. Because of the lower repulsion of the cyanide ion than that of the halogen atom as mentioned above, the M−M distances of **1** and **2** should be shorter than those of **4** and **5**. Figure 3 displays that **1** possesses a $\sigma(p_z)$ bonding HOMO and **2**, **4**, and **5** have the HOMOs with $\delta(d_{x^2-y^2})$ character. The stronger $\sigma(p_z)$ bonding results in the shorter M−M distance for **1**. For the HOMOs with $\delta(d_{x^2-y^2})$ charactes of **4** and **5**, coordination of the halogen atom to platinum increases the electrons of bonding HOMOs, contracting the Pt−Pt distance. In contrast, the repulsion of the halogen

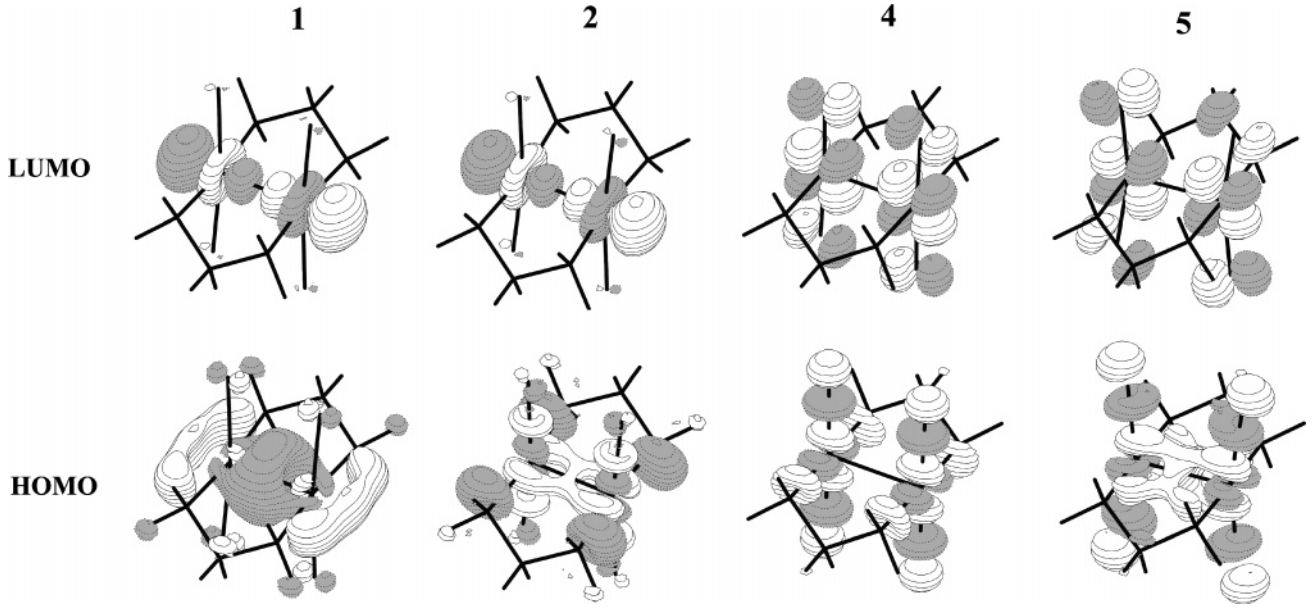

Figure 3. Electron density diagrams of HOMO and LUMO for **1**, **2**, **4**, and **5** under UMP2 calculations.

atoms lengthens the Pt−Pt separation. For the face-to-face square-planar complexes (**4** and **5**), halogen atoms directly coordinate to platinum(II) while the repulsion interaction occurs between adjacent halogen atoms (3.267 Å for **4** and 3.699 Å for **5**). Thus, the stronger donating ability of the bromine atom leads to a slightly shorter Pt−Pt distance for **4** than **5**.

In this work, we predict that the emission energy that refers to the difference of the total energies between the triplet excited state and the singlet ground state with the same excited-state structure. **1**, **2**, **4**, and **5** give rise to lowest energy phosphorescent emissions at 2.66 (467), 2.30 (539), 1.65 (751), and 1.49 eV (831 nm), respectively. Compared with experimental values available, the UMP2 method slightly underestimates the emission energy. For example, the emission energy (2.66 eV/467 nm) of **1** is lower than experimental 2.76 eV/450 nm of *trans*-$[Pt_2(CN)_4(PCy_2CH_2PCy_2)_2]$ in the solid state at room temperature;[12] the emission energy of **2** underestimates by ca. 0.17 eV relative to 2.47 eV (503 nm) of *trans*-$[Pd_2(CN)_4(PCy_2CH_2PCy_2)_2]$ observed in the solid state at 77 K.[14] The UMP2 calculations show that the ^3A_u excited state of **1** can give the $\sigma(p_z) \rightarrow \sigma^*(d_{z^2})$ (HOMO → LUMO) phosphorescent emission, while those of **2** and **4**/**5** contribute to the lowest energy $\delta(d_{x^2-y^2}) \rightarrow \sigma^*(d_{z^2})$ and $\delta(d_{x^2-y^2}) \rightarrow \pi^*(d_{xz})$ transitions, respectively (Figure 3).

In addition, we carried out frequency calculations on **1**, **2**, **4**, and **5** for the lowest energy triplet excited states to characterize the M(II)−M(II) interactions. Because the HOMOs in their triplet excited states all have bonding properties, the excited-state M−M stretching frequencies should be higher than those of the ground states. Through vibrational-mode analyses, the calculated 140 cm^{-1} frequency of **1** in the $^3[\sigma^*(d_{z^2})\sigma(p_z)]$ excited state was attributed to the Pt−Pt stretching frequency, much higher than the 94 cm^{-1} one in the ground state. This suggests that the interaction between the two Pt atoms is weak in the ground state (3.069 Å Pt−Pt distance) but strongly enhanced in the triplet excited state (2.794 Å Pt−Pt distance). The excited-state Pt−Pt stretching frequency of **1** agrees well with the 145 cm^{-1} for *trans*-$[Pt_2(CN)_4(PCy_2CH_2PCy_2)_2]^*$ estimated by the resonance Raman spectra[12] and is comparable to the excited Pt−Pt frequencies, 146 cm^{-1} for $\{[Pt_2(pcp)_4]^{4-}\}^*$ (pcp = $P_2O_4CH_4^{2-}$)[48] and 155 cm^{-1} for $\{[Pt_2(pop)_4]^{4-}\}^*$[1,44,45a,48] and to the experimental d^7-d^7 stretching frequencies, 158 cm^{-1} for $[Pt_2(pop)_4Cl_2]^{4-}$,[1,45,49] 134 cm^{-1} for $[Pt_2(pop)_4Br_2]^{4-}$,[1,45c,49] and 156 cm^{-1} for $[Pt_2(pop)_4CH_3I]^{4-}$.[1,45c] Similarly, the excited-state M−M frequencies of **2**, **3**, and **5** (166, 95, and 84 cm^{-1}, respectively) also increase relative to those in their ground states. The present studies demonstrate that the M(II)−M(II) stretching frequency is correlated with M−M distance, namely, stronger frequency, shorter distance. In Supporting Information Table 15, we summarized the calculated M−M distances and stretching frequencies in the ground and lowest energy triplet excited states for a series of binuclear d^8 complexes from MP2 and UMP2 calculations, respectively. The plot of the M−M distances versus stretching frequencies in Figure 4 intuitively illustrates that the M−M distances are linearly correlated with the M−M stretching frequencies for binuclear d^8 complexes.

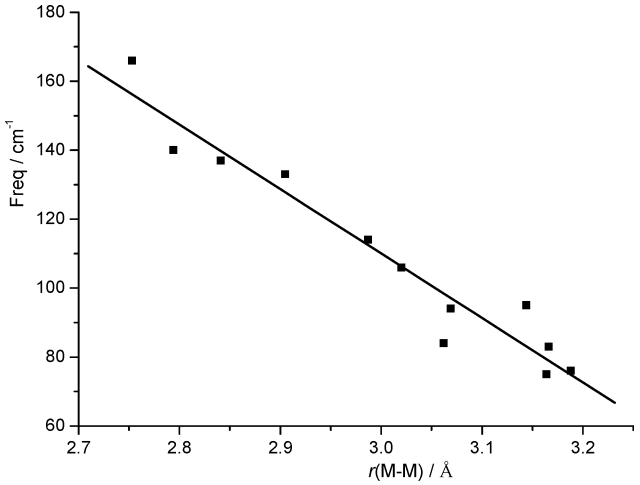

Figure 4. Plot of M−M distances versus stretching frequencies in the ground and lowest-energy triplet excited states for a series of binuclear d^8 complexes (Supporting Information, Table 15) under MP2 and UMP2 calculations, respectively.

4. Conclusions

We explored the ground- and excited-state properties of binuclear d^8 complexes **1**−**5** at the MP2 and UMP2 levels. In the ground state, the calculated M(II)−M(II) distances range from 3.02 to 3.17 Å. Though the slightly shorter distance than

the van der Waals contacts of 3.2 Å implies a weak bonding interaction between the two metal atoms, frequency calculations demonstrate that the weak metal−metal interaction in **1**, **2**, **4**, and **5** is bonding in nature but in **3** is not. This agrees with the experimental results.[12,14] Upon excitation, the metal−metal distances shorten by ca. 0.28, 0.27, 0.02, and 0.10 Å for **1**, **2**, **4**, and **5**, respectively. Enhancement of the metal−metal interaction is related to promotion of electrons into bonding σ-(p_z) or $\delta(d_{x^2-y^2})$ orbitals. The present calculations on binuclear d^8 complexes in the ground and triplet excited states reveal that the M−M distances are linearly correlated with the M−M stretching frequencies.

To rationalize spectroscopic properties, the TD-DFT method associated with the polarized continuum model (PCM) was performed to predict absorption spectra **1**−**5** as well as mononuclear d^8 complexes **6**−**8** in CH_2Cl_2 solution. For **6**−**8**, the calculated 233, 218, and 246 nm absorptions were assigned as spin-allowed $d_{z^2} \rightarrow p_z$ transitions, respectively, while the σ^*-(d_{z^2}) → $\sigma(p_z)$ transition absorptions of **1**−**3** were calculated at 338, 296, and 314 nm. With respect to analogous mononuclear d^8 complexes, the metal−metal interaction results in a large red shift of absorption wavelength for the binuclear d^8 complexes. Relative to **1** with unsaturated CN^- donors, introduction of saturated halogen donors into **4** and **5** changes their HOMO and LUMO character, which leads to the lower energy d → d transition absorptions in platinum(II) halide complexes.

UMP2 calculations predict the lowest energy phosphorescent emissions of **1**, **2**, **4**, and **5** at 467, 539, 751, and 831 nm, respectively. The first two are in agreement with the experimental 450 nm emission of *trans*-$[Pt_2(CN)_4(PCy_2CH_2PCy_2)_2]$ and 503 nm of *trans*-$[Pd_2(CN)_4(PCy_2CH_2PCy_2)_2]$ in the solid state, respectively. It is shown that the ^3A_u excited state of **1** can give the $\sigma(p_z) \rightarrow \sigma^*(d_{z^2})$ phosphorescent emission, while those of **2** and **4**/**5** contribute to the lowest energy $\delta(d_{x^2-y^2}) \rightarrow \sigma^*(d_{z^2})$ and $\delta(d_{x^2-y^2}) \rightarrow \pi^*(d_{xz})$ transitions, respectively. These results are also supported by such TD-DFT calculations.

Acknowledgment. This work was supported by the National Natural Science Foundation of China (Nos. 20173021, 20301006, 20573042, 20671032), the Natural Science Foundation of Heilongjiang Province of China (No. B200601), and the Science Foundation for Excellent Youth of Heilongjiang University of China (2007).

Supporting Information Available: Tables of absorptions for **2**−**5**, **7**, and **8**; tables of partial molecular orbital contributions (%) for **1**−**8** in CH_2Cl_2 solution under TD-DFT (B3LYP) calculations; table of calculated M−M distances and stretching frequencies for a series of binuclear d^8 complexes; figure of the energy-level diagram of **1** and **6**. This material is available free of charge via the Internet at http://pubs.acs.org.

References and Notes

(1) Zipp, A. P. *Coord. Chem. Rev.* **1988**, *84*, 47−83.

(2) Roundhill, D. M.; Gray, H. B.; Che, C.-M. *Acc. Chem. Res.* **1989**, *22*, 55−61.

(3) (a) Yam, V. W.-W.; Wong, K. M.-C.; Zhu, N. *J. Am. Chem. Soc.* **2002**, *124*, 6506−6507. (b) Yam, V. W.-W.; Tang, R. P.-L.; Wong, K. M.-C.; Lu, X.-X.; Cheung, K.-K.; Zhu, N. *Chem. Eur. J.* **2002**, *8*, 4066−4076. (c) Lai, S.-W.; Lam, H.-W.; Lu, W.; Cheung, K.-K.; Che, C.-M. *Organometallics* **2002**, *21*, 226−234. (d) McMillin, D. R.; Moore, J. J. *Coord. Chem. Rev.* **2002**, *229*, 113−121. (e) Neve, F.; Crispini, A.; Pietro, C. D.; Campagna, S. *Organometallics* **2002**, *21*, 3511−3518.

(4) (a) Jain, V. K.; Jain, I. *Coord. Chem. Rev.* **2005**, *249*, 3075−3197. (b) Hummel, H.-U. *Transition Met. Chem.* **1987**, *12*, 172−174. (c) Janka, M.; Anderson, G. K.; Rath, N. P. *Organometallics* **2000**, *19*, 5071−5076. (d) Kunkely, H.; Vogler, A. *J. Am. Chem. Soc.* **1990**, *112*, 5625−5627. (e) Cera, M.; Cerrada, C.; Laguna, M.; Mata, J. A.; Teruel, H. *Organometallics* **2002**, *21*, 121−126. (f) Richmond, M. K.; Scott, S. L.; Yap, G. P. A.; Alper, H. *Organometallics* **2002**, *21*, 3395−3400. (g) Pamplin, C. B.; Rettig, S. J.; Patrick, B. O.; James, B. R. *Inorg. Chem.* **2003**, *42*, 4117−4126.

(5) (a) Chan, S.-C.; Chan, M. C. W.; Wang, Y.; Che, C.-M.; Cheung, K.-K.; Zhu, N. *Chem. Eur. J.* **2001**, *7*, 4180−4190. (b) Che, C.-M.; He, L.-Y.; Poon, C.-K.; Mak, T. C. W. *Inorg. Chem.* **1989**, *28*, 3081−3083.

(6) Kato, M.; Kosuge, C.; Morii, K.; Ahn, J. S.; Kitagawa, H.; Mitani, T.; Matsushita, M.; Kato, T.; Yano, S.; Kimura, M. *Inorg. Chem.* **1999**, *38*, 1638−1641.

(7) Pomestchenko, I. E.; Luman, C. R.; Hissler, M.; Ziessel, R.; Castellano, F. N. *Inorg. Chem.* **2003**, *42*, 1394−1396.

(8) Hissler, M.; McGarrah, J. E.; Connick, W. B.; Geiger, D. K.; Cummings, S. D.; Eisenberg, R. *Coord. Chem. Rev.* **2000**, *208*, 115−137.

(9) (a) Miskowski, V. M.; Houlding, V. H. *Inorg. Chem.* **1991**, *30*, 4446−4452. (b) Miskowski, V. M.; Houlding, V. H. *Inorg. Chem.* **1989**, *28*, 1529−1533. (c) Houlding, V. H.; Miskowski, V. M. *Coord. Chem. Rev.* **1991**, *111*, 145−152.

(10) Wong, K. M.-C.; Hui, C.-K.; Yu, K.-L.; Yam, W. W.-W. *Coord. Chem. Rev.* **2002**, *229*, 123−132.

(11) Hassan, F. S. M.; Markham, D. P.; Pringle, P. G.; Shaw, B. L. *J. Chem. Soc., Dalton Trans.* **1985**, 279−283.

(12) Xia, B.-H.; Che, C.-M.; Phillips, D. L.; Leung, K.-H.; Cheung, K.-K. *Inorg. Chem.* **2002**, *41*, 3866−3875.

(13) Che, C.-M.; Yam, V. W.-W.; Wong, W.-T.; Lai, T.-F. *Inorg. Chem.* **1989**, *28*, 2908−2910.

(14) Xia, B.-H.; Che, C.-M.; Zhou, Z.-Y. *Chem. Eur. J.* **2003**, *9*, 3055−3064.

(15) Yip, H.-K.; Lai, T.-F.; Che, C.-M. *J. Chem. Soc., Dalton Trans.* **1991**, 1639−1641.

(16) Pan, Q.-J.; Zhang, H.-X. *Chem. Phys. Letters.* **2004**, *294*, 155−160.

(17) Mann, K. R.; Gordon, J. G., II; Gray, H. B. *J. Am. Chem. Soc.* **1975**, *97*, 3553−3555.

(18) (a) Novozhilova, I. V.; Volkov, A. V.; Coppens, P. *J. Am. Chem. Soc.* **2003**, *125*, 1079−1087. (b) Stoyanov, S. R.; Villegas, J. M.; Rillema, D. P. *J. Phys. Chem. B.* **2004**, *108*, 12175−12180.

(19) Kim, C. D.; Pillet, S.; Wu, G.; Fullagar, W. K.; Coppens, P. *Acta Crystallogr.* **2002**, *A58*, 133−137.

(20) (a) Fu, W.-F.; Chan, K.-C.; Miskowski, V. M.; Che, C.-M. *Angew. Chem., Int. Ed.* **1999**, *38*, 2783−2785. (b) Fu, W.-F.; Chan, K.-C.; Cheung, K.-K.; Che, C.-M. *Chem. Eur. J.* **2001**, *7*, 4656−4664. (c) Phillips, D. L.; Che, C.-M.; Leung, K. H.; Mao, Z.; Tse, M.-C. *Coord. Chem. Rev.* **2005**, *249*, 1476−1490.

(21) (a) Fernández, E. J.; López de Luzuraga, J. M.; Monge, M.; Rodríguez, M. A.; Crespo, O.; Gimeno, M. C.; Laguna, A.; Jones, P. G. *Inorg. Chem.* **1998**, *37*, 6002−6006. (b) King, C.; Wang, J.-C.; Khan, Md. N. I.; Fackler, J. P., Jr. *Inorg. Chem.* **1989**, *28*, 2145−2149. (c) Catalano, V. J.; Moore, A. L. *Inorg. Chem.* **2005**, *44*, 6558−6566.

(22) (a) Pan, Q.-J.; Zhang, H.-X. *Inorg. Chem.* **2004**, *43*, 593−601. (b) Pan, Q.-J.; Zhang, H.-X. *J. Phys. Chem. A* **2004**, *108*, 3650−3661. (c) Pan, Q.-J.; Zhang, H.-X. *Eur. J. Inorg. Chem.* **2006**, 1050−1059.

(23) Novozhilova, I. V.; Volkov, A. V.; Coppens, P. *Inorg. Chem.* **2004**, *43*, 2299−2307.

(24) (a) Novoa, J. J.; Aullón, G.; Alemany, P.; Alvarez, S. *J. Am. Chem. Soc.* **1995**, *117*, 7169−7171. (b) Aullón, G.; Alemany, P.; Alvarez, S. *Inorg. Chem.* **1996**, *35*, 5061−5067. (c) Cotton, F. A.; Matusz, M.; Poli, R.; Feng, X. *J. Am. Chem. Soc.* **1988**, *110*, 1144−1154.

(25) (a) Solar, J. M.; Ozkan, M. A.; Isci, H.; Mason, W. R. *Inorg. Chem.* **1984**, *23*, 758−764. (b) Solar, J. M.; Rogers, R. D.; Mason, W. R. *Inorg. Chem.* **1984**, *23*, 373−377. (c) Roberts, D. A.; Mason, W. R.; Geoffroy, G. L. *Inorg. Chem.* **1981**, *20*, 789−796. (d) Isci, H.; Mason, W. R. *Inorg. Chem.* **1975**, *14*, 905−912.

(26) (a) Mason, W. R., III; Gray, H. B. *J. Am. Chem. Soc.* **1968**, *90*, 5721−5729. (b) Cowman, C. D.; Gray, H. B. *Inorg. Chem.* **1976**, *15*, 2823−2824. (c) Basch, H.; Gray, H. B. *Inorg. Chem.* **1967**, *6*, 365−369.

(27) Fernández, E. J.; Gimeno, M. C.; Jones, P. G.; Laguna, A.; Laguna, M.; López de Luzuriaga, J. M.; Rodriguez, M. A. *Chem. Ber.* **1995**, *128*, 121−124.

(28) Møller, C.; Plesset, M. S. *Phys. Rev.* **1934**, *46*, 618−622.

(29) (a) Casida, M. E.; Jamorski, C.; Casida, K. C.; Salahub, D. R. *J. Chem. Phys.* **1998**, *108*, 4439−4449. (b) Jamorski, C.; Casida, M. E.; Salahub, D. R. *J. Chem. Phys.* **1996**, *104*, 5134−5147.

(30) Statmann, R. E.; Scuseria, G. E. *J. Chem. Phys.* **1998**, *109*, 8218−8224.

(31) Bauernschmitt, R.; Ahlrichs, R. *Chem. Phys. Lett.* **1996**, *256*, 454−464.

(32) Matsuzawa, N. N.; Ishitani, A.; Dixon, D. A.; Uda, T. *J. Phys. Chem. A* **2001**, *105*, 4953−4962.

(33) (a) Pople, J. A.; Gill, P. M. W.; Johnson, B. G. *Chem. Phys. Lett.* **1992**, *199*, 557−560. (b) Johnson, B. G.; Frisch, M. J. *J. Chem. Phys.* **1994**, *100*, 7429−7442.

(34) (a) Miertuš, S.; Scrocco, E.; Tomasi, J. *J. Chem. Phys.* **1981**, *55*, 117−129. (b) Cancès, E.; Mennucci, B.; Tomasi, J. *J. Chem. Phys.* **1997**, *107*, 3032−3041. (c) Barone, V.; Cossi, M.; Tomasi, J. *J. Comput. Chem.* **1998**, *19*, 404−417.

(35) (a) Wadt, W. R.; Hay, P. J. *J. Chem. Phys.* **1985**, *82*, 284−298. (b) Hay, P. J.; Wadt, W. R. *J. Chem. Phys.* **1985**, *82*, 299−310.

(36) (a) Pyykkö, P.; Runeberg, N.; Mendizabal, F. *Chem. Eur. J.* **1997**, *3*, 1451−1457. (b) Pyykkö, P.; Mendizabal, F. *Chem. Eur. J.* **1997**, *3*, 1458−1465. (c) Pyykkö, P.; Mendizabal, F. *Inorg. Chem.* **1998**, *37*, 3018−3025. (d) Pyykkö, P. *Chem. Rev.* **1997**, *97*, 597−636. (e) Pyykkö, P.; Zhao, Y.-F. *Angew. Chem., Int. Ed.* **1991**, *30*, 604−605. (f) Pyykkö, P. *Science* **2000**, *290*, 64−65.

(37) Frisch, M. J.; Trucks, G. W.; Schlegel, H. B.; Scuseria, G. E.; Robb, M. A.; Cheeseman, J. R.; Montgomery, J. A., Jr.; Vreven, T.; Kudin, K. N.; Burant, J. C.; Millam, J. M.; Iyengar, S. S.; Tomasi, J.; Barone, V.; Mennucci, B.; Cossi, M.; Scalmani, G.; Rega, N.; Petersson, G. A.; Nakatsuji, H.; Hada, M.; Ehara, M.; Toyota, K.; Fukuda, R.; Hasegawa, J.; Ishida, M.; Nakajima, T.; Honda, Y.; Kitao, O.; Nakai, H.; Klene, M.; Li, X.; Knox, J. E.; Hratchian, H. P.; Cross, J. B.; Adamo, C.; Jaramillo, J.; Gomperts, R.; Stratmann, R. E.; Yazyev, O.; Austin, A. J.; Cammi, R.; Pomelli, C.; Ochterski, J. W.; Ayala, P. Y.; Morokuma, K.; Voth, G. A.; Salvador, P.; Dannenberg, J. J.; Zakrzewski, V. G.; Dapprich, S.; Daniels, A. D.; Strain, M. C.; Farkas, O.; Malick, D. K.; Rabuck, A. D.; Raghavachari, K.; Foresman, J. B.; Ortiz, J. V.; Cui, Q.; Baboul, A. G.; Clifford, S.; Cioslowski, J.; Stefanov, B. B.; Liu, G.; Liashenko, A.; Piskorz, P.; Komaromi, I.; Martin, R. L.; Fox, D. J.; Keith, T.; Al-Laham, M. A.; Peng, C. Y.; Nanayakkara, A.; Challacombe, M.; Gill, P. M. W.; Johnson, B.; Chen, W.; Wong, M. W.; Gonzalez, C.; Pople, J. A. *Gaussian 03*, Revision B.03; Gaussian, Inc.: Pittsburgh PA, 2003.

(38) Tang, S. S.; Chang, C.-P.; Lin, I. J. B.; Liou, L.-S.; Wang, J.-C. *Inorg. Chem.* **1997**, *36*, 2294−2300.

(39) (a) Heinrich, D. D.; Wang, J.-C.; Fackler, J. P., Jr. *Acta Crystallogr.* **1990**, *C46*, 1444−1447. (b) Lee, Y. A.; McGarrah, J. E.; Lachicotte, R. J.; Eisenberg, R. *J. Am. Chem. Soc.* **2002**, *124*, 10662−10663. (c) Mansour, M. A.; Connick, W. B.; Lachicotte, R. J.; Gysling, H. J.; Eisenberg, R. *J. Am. Chem. Soc.* **1998**, *120*, 1329−1330.

(40) Bondi, A. *J. Phys. Chem.* **1964**, *68*, 441−451.

(41) Stoyanov, S. R.; Villegas, J. M.; Rillema, D. P. *Inorg. Chem.* **2003**, *42*, 7852−7860.

(42) (a) Barone, V.; De Biani, F. F.; Ruiz, E.; Sieklucka, B. *J. Am. Chem. Soc.* **2001**, *123*, 10742−10743. (b) Fernández, E. J.; Jones, P. G.; Laguna, A.; López-de-Luzuriaga, J. M.; Monge, M.; Pérez, J.; Olmos, M. E. *Inorg. Chem.* **2002**, *41*, 1056−1063.

(43) (a) Sweeney, R. J.; Harvey, E. L.; Gray, H. B. *Coord. Chem. Rev.* **1990**, *105*, 23−24. (b) Che, C.-M.; Butler, L. G.; Gray, H. B. *J. Am. Chem. Soc.* **1981**, *103*, 7796−7797. (c) Pettijohn, C. N.; Jochnowitz, E. B.; Chuong, B.; Nagle, J. K.; Vogler, A. *Coord. Chem. Rev.* **1998**, *171*, 85−92. (d) Bojan, V. R.; Fernandez, E. J.; Laguna, A.; Lopez-de-Luzuriaga, J. M.; Monge, M.; Olmos, M. E.; Silvestru, C. *J. Am. Chem. Soc.* **2005**, *127*, 11564−11565.

(44) (a) Shimizu, Y.; Tanaka, Y.; Azumi, T. *J. Phys. Chem.* **1985**, *89*, 1372−1374. (b) Rice, S. F.; Gray, H. B. *J. Am. Chem. Soc.* **1983**, *105*, 4571−4575.

(45) (a) Che, C.-M.; Butler, L. G.; Gray, H. B.; Crooks, R. M.; Woodruff, W. H. *J. Am. Chem. Soc.* **1983**, *105*, 5492−5494. (b) Stein, P.; Dickson, M. K.; Roundhill, D. M. *J. Am. Chem. Soc.* **1983**, *105*, 3489−3494.

(46) Isci, H.; Mason, W. R. *Inorg. Chem.* **1985**, *24*, 1761−1765.

(47) (a) McKeage, M. J.; Maharaj, L.; Berners-Price, S. J. *Coord. Chem. Rev.* **2002**, *232*, 127−135. (b). Navarro, M.; Pérez, H.; Sánchez−Delgado, R. A. *J. Med. Chem.* **1997**, *40*, 1937−1939. (c). Corey, E. J.; Mahrotra, M. M.; Khan, A. U. *Science* **1987**, *236*, 68−69.

(48) King, C.; Auerbach, R. A.; Fronczek, F. R.; Roundhill, D. M. *J. Am. Chem. Soc.* **1986**, *108*, 5626−5627.

(49) Che, C.-M.; Schaefer, W. P.; Gray, H. B.; Dickson, M. K.; Stein, P. B.; Roundhill, D. M. *J. Am. Chem. Soc.* **1982**, *104*, 4253−4255.